Supporting Information: Spectroscopic detection and characterization of cyanooxomethylium, $NCCO^+$

Marcel Bast,[†] Julian Böing,[†] Thomas Salomon,[†] Eline Plaar,[†] Igor Savić,[‡] Mathias Schäfer,[¶] Oskar Asvany,[†] Stephan Schlemmer,[†] and Sven Thorwirth[*,†]

†*I. Physikalisches Institut der Universität zu Köln, Köln, Germany*

‡*University of Novi Sad, Faculty of Sciences, Department of Physics, Novi Sad 21000, Serbia*

¶*Institute of Organic Chemistry, Department of Chemistry, University of Cologne, Greinstrasse 4, 50937 Köln, Germany*

E-mail: sthorwirth@ph1.uni-koeln.de

Contents

Quantum-chemical calculations

Structural calculations

Table S1: CCSD(T) structural parameters of $NCCO^+$ (in Å), center-of-mass-frame dipole moments (in D), and nitrogen nuclear quadrupole coupling constants eQq(N) (in MHz) calculated using various basis sets.

Basis set	r_{N-C}	r_{C-C}	r_{C-O}	μ	eQq
cc-pVTZ	1.1736	1.3738	1.1228	1.605	−5.771
aug-cc-pVTZ	1.1733	1.3745	1.1227	1.594	−5.763
cc-pVQZ	1.1698	1.3723	1.1188	1.604	−5.953
aug-cc-pVQZ	1.1700	1.3724	1.1190	1.598	−5.949
ANO1	1.1735	1.3719	1.1221	1.593	−5.807
ANO2	1.1697	1.3715	1.1188	1.604	−5.963
cc-pwCVTZ	1.1696	1.3714	1.1191	1.625	−5.798
aug-cc-pwCVTZ	1.1697	1.3713	1.1195	1.609	−5.791
cc-pwCVQZ	1.1668	1.3692	1.1163	1.619	−5.880
aug-cc-pwCVQZ	1.1670	1.3694	1.1165	1.613	−5.875

Table S2: Internal coordinates for the bare $NCCO^+$ ion in comparison against the T-shaped Ne-complex calculated at the fc-CCSD(T)/aug-cc-pVTZ level. Bond lengths are given in Å, angles in degrees.

```
NCCO+                          NCCO+, T-shaped Ne-cluster
N                              N
C 1 r1                         C 1 r1
X 2 rd 1 a90                   X 2 rd 1 a90
C 2 r2 3 a90 1 d180            C 2 r2 3 a1 1 d180
X 4 rd 2 a90 3 d0              X 4 rd 2 a90 3 d0
O 4 r3 5 a90 2 d180            O 4 r3 5 a2 2 d180
                               NE 6 r4 4 a3 5 d0

r1   =        1.17333          r1   =        1.17310
rd   =        1.00000          rd   =        1.00000
a90  =       90.00000          a90  =       90.00000
r2   =        1.37453          r2   =        1.37470
                ...              a1   =       90.41725
d180 =      180.00000          d180 =      180.00000
d0   =        0.00000          d0   =        0.00000
r3   =        1.12266          r3   =        1.12252
                ...              a2   =       90.45498
                ...              r4   =        3.13242
                ...              a3   =       65.46457
```

Table S3: Rotation-vibration interaction constants α_i, and ℓ-type doubling constants q_i of $NCCO^+$ calculated at the fc-CCSD(T)/ANO2 level of theory.

Mode	α_i [MHz]	q_i [MHz]
$\nu_1(\sigma)$	24.434	$\cdots$
$\nu_2(\sigma)$	17.002	$\cdots$
$\nu_3(\sigma)$	11.738	$\cdots$
$\nu_4(\pi)$	−9.675	3.363
$\nu_5(\pi)$	−22.732	7.751

Empirical scaling of $NCCO^+$ rotational constant

Table S4: Empirical scaling of $NCCO^+$ rotational constant from different molecular calibrators.

Calibrator	B_e[a] [MHz]	ΔB_0[b] [MHz]	$B_{0,calc}$ [MHz]	$B_{0,exp}$ [MHz]	Ref.	B_{exp}/B_{calc}	$B_0(NCCO^+, BE)$ [MHz]	$B_{0,BE} - B_{0,exp}$ [MHz]
NCCN	4703.906	0.132	4703.774	4709.386	1	1.00119	4564.206	0.426
CNCN	5167.891	−1.025	5168.916	5174.136	2	1.00101	4563.371	−0.409
C_3O	4791.246	−14.880	4806.126	4810.886	3	1.00099	4563.282	−0.498
C_3N^-	4849.673	2.377	4847.296	4851.622	4	1.00089	4562.835	−0.945
C_4H^-	4651.521	1.309	4650.212	4654.945	5	1.00102	4563.407	−0.373
HC_3N	4544.861	1.783	4543.078	4549.059	6	1.00132	4564.769	0.989
HCCNC	4963.987	1.573	4962.414	4967.838	7	1.00109	4563.749	−0.031
HC_3O^+	4453.556	−1.691	4455.247	4460.589	8	1.00120	4564.233	0.453
$NCCNH^+$	4430.646	−1.669	4432.315	4438.012	9	1.00129	4564.626	0.846
HC_3NH^+	4323.167	0.099	4323.266	4328.997	9	1.00133	4564.810	1.030
$HCCNCH^+$	4660.996	2.256	4658.741	4664.432	10	1.00122	4564.336	0.556
$NCCO^+$	4554.302	−4.465	4558.767	4563.780		1.00110	···	···

[a] ae-CCSD(T)/cc-pwCVQZ. [b] fc-CCSD(T)/ANO1.

Mass spectra

FELion: $NCCO^+$, pyruvonitrile

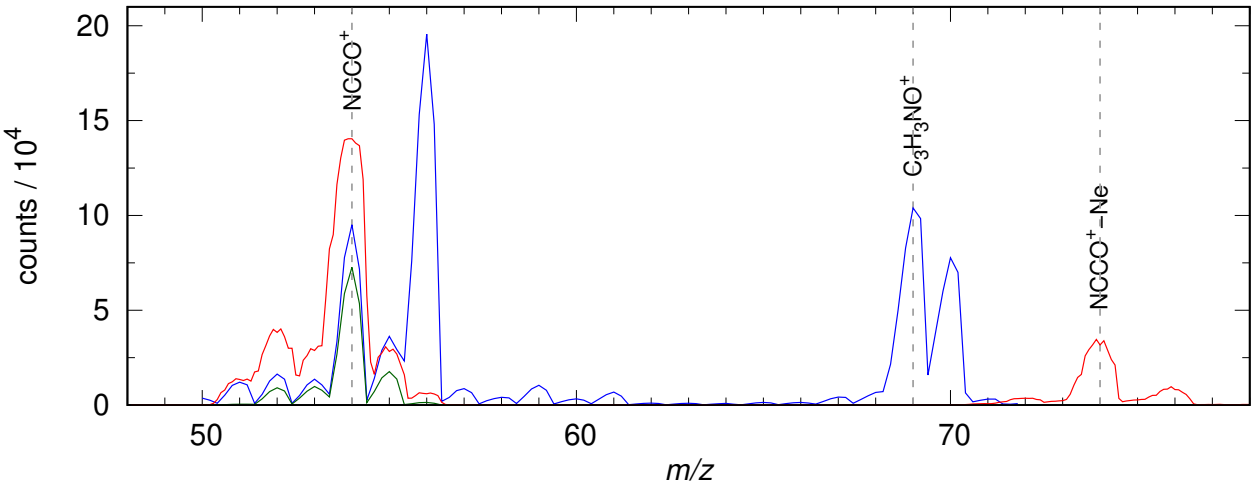

Figure S1: Mass spectra of precursor pyruvonitrile (acetyl cyanide, C_3H_3NO), produced in a storage ion source (SIS) via electron bombardment using an electron energy of about 55 eV. Blue trace: First quadrupole mass selector (QP I) of 4 K 22-pole ion trap apparatus FELion is used non-mass-selective as an ion guide. Ions pass through the ion trap without being trapped, get analyzed in the second quadrupole (QP II) and are detected subsequently. Green trace: Similar conditions as for blue trace, but QP I is used as a mass selector and only transmits around $m/z = 54$. Red trace: Mass selected ions (via QP I) are trapped and cooled down to a nominal temperature of 7 K by a 3:1 He:Ne mixture, while also forming $NCCO^+$–Ne clusters ($m/z = 74$) in the trap. Masses of precursor, ions of interest and their corresponding Ne–clusters are highlighted by vertical dashed gray lines.

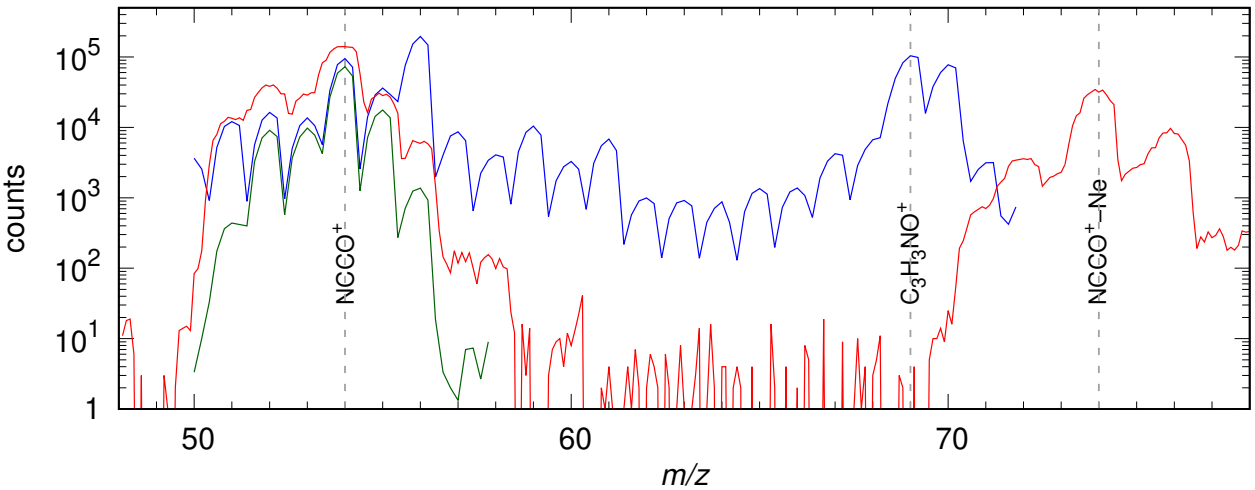

Figure S2: Same data as above (Fig. S1), using a logarithmic plot of the counts.

COLtrap II: $NCCO^+$, methyl cyanoformate

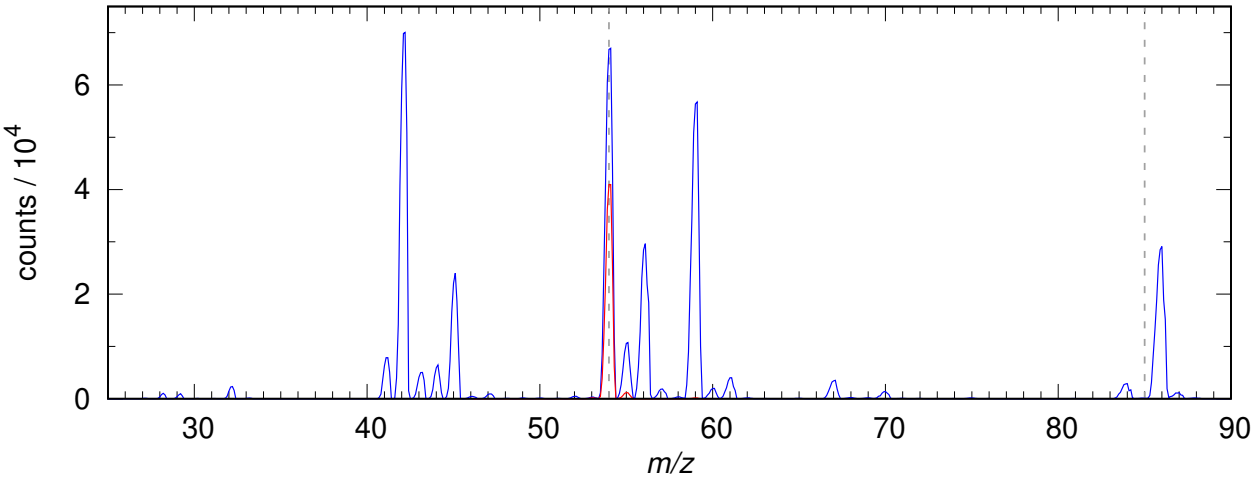

Figure S3: Mass spectra of precursor methyl cyanoformate ($CH_3OC(O)CN$), produced in the SIS of the COLtrap II apparatus by electron bombardment using an electron energy of about 65 eV. Blue trace: QP I is used non-mass-selective as an ion guide. Ions are trapped and cooled down to nominal trap temperature of 42(2) K by a cold He pulse and continuous flow of N_2, extracted, analyzed in QP II and detected subsequently. Red trace: Same conditions as for blue trace, but mass selection (via QP I) only allows ions around $m/z = 54$ ($NCCO^+$) to pass. Masses of precursor and ions of interest are highlighted by vertical dashed gray lines.

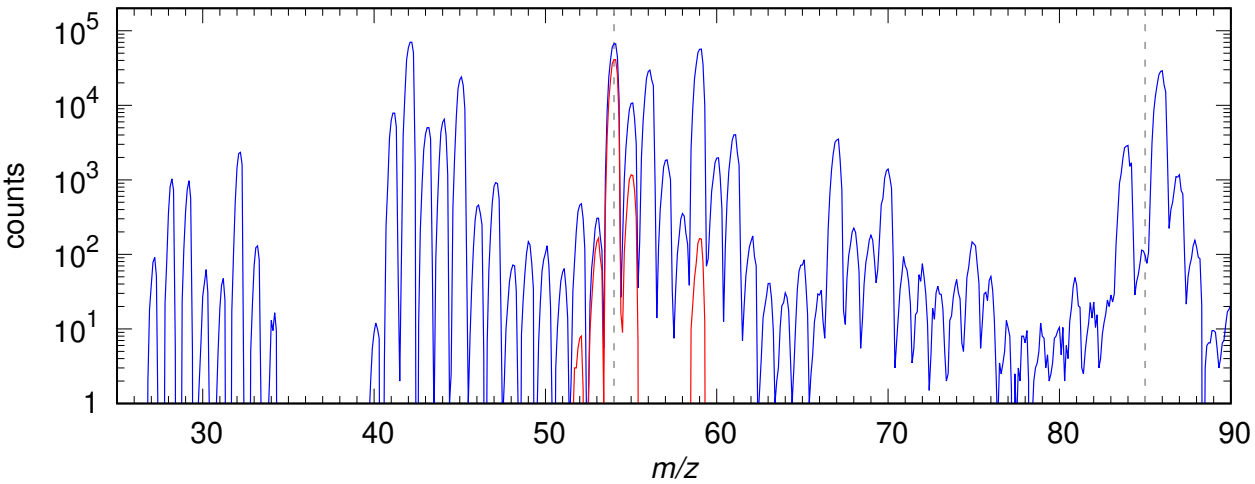

Figure S4: Same data as above (Fig. S3), using a logarithmic plot of the counts.

IR-LOS studies: IR spectra, Boltzmann Plot

Infrared (IR) leak-out (LO) spectra of ro-vibrational transitions of $NCCO^+$ recorded with the 10 K ion trap apparatus COLtrap II, using a quantum cascade laser (QCL, Daylight Solutions MHF 1961 - 2205 cm^{-1}) are shown in Fig. S5. The laser scanning speed was chosen such to ensure an accurate depiction of the line shape of the ro-vibrational transitions. Similar off-resonance background LO rates were used throughout the entire measuring range to achieve comparable IR intensities of all individual transitions. Assuming saturation effects to be negligible, the rotational temperature of $NCCO^+$ in the ion trap was determined via the line intensity distribution in the $P-$ and $R-$branches of the ν_2 band using a Boltzmann plot (see Fig. S6). The smooth linear trend yields $T_{rot,\,P} = 51.2(9)$ K from P-branch data and $T_{rot,\,R} = 48.8(16)$ K from R-branch data, resulting in an average $T_{rot} = 50.0(9)$ K. The excellent agreement of the (linear) Boltzmann-like intensity distribution of the pure experimental data without any normalization necessary - both in the P- and the R-branch - suggests no dependence of the rotational state J on the LO process. The collisional temperature T_{col} of the ions and their neutral collision partner Neon ($T_{neutral} = 42(2)$ K), can be derived from the collisional kinetic energy in the center-of-mass system: $T_{col} = \frac{(m_{ion}\ T_{neutral}\ +\ m_{neutral}\ T_{ion})}{(m_{ion}\ +\ m_{neutral})}$. Assuming the rotational temperature of the ions to be equal to the effective collisional temperature T_{col}, a quite reliable ion temperature T_{ion} can be calculated as 65 K. Compared to the nominal trap temperature of 42(2) K, this shows a somewhat increased temperature of the ions, indicating heating effects of collisions under the influence of the radio frequency (RF) field of the trap.[11] The corresponding, experimentally observed line width $FWHM_{total}$ of about 60 MHz (0.002 cm^{-1}) is primarily composed of Doppler broadening and the laser linewidth, resulting in: $FWHM_{total} = \sqrt{FWHM_{ion}^2 + FWHM_{laser}^2}$. Accordingly, the IR data lead to an experimental laser linewidth of 40 MHz, which aligns with the QCL specifications.

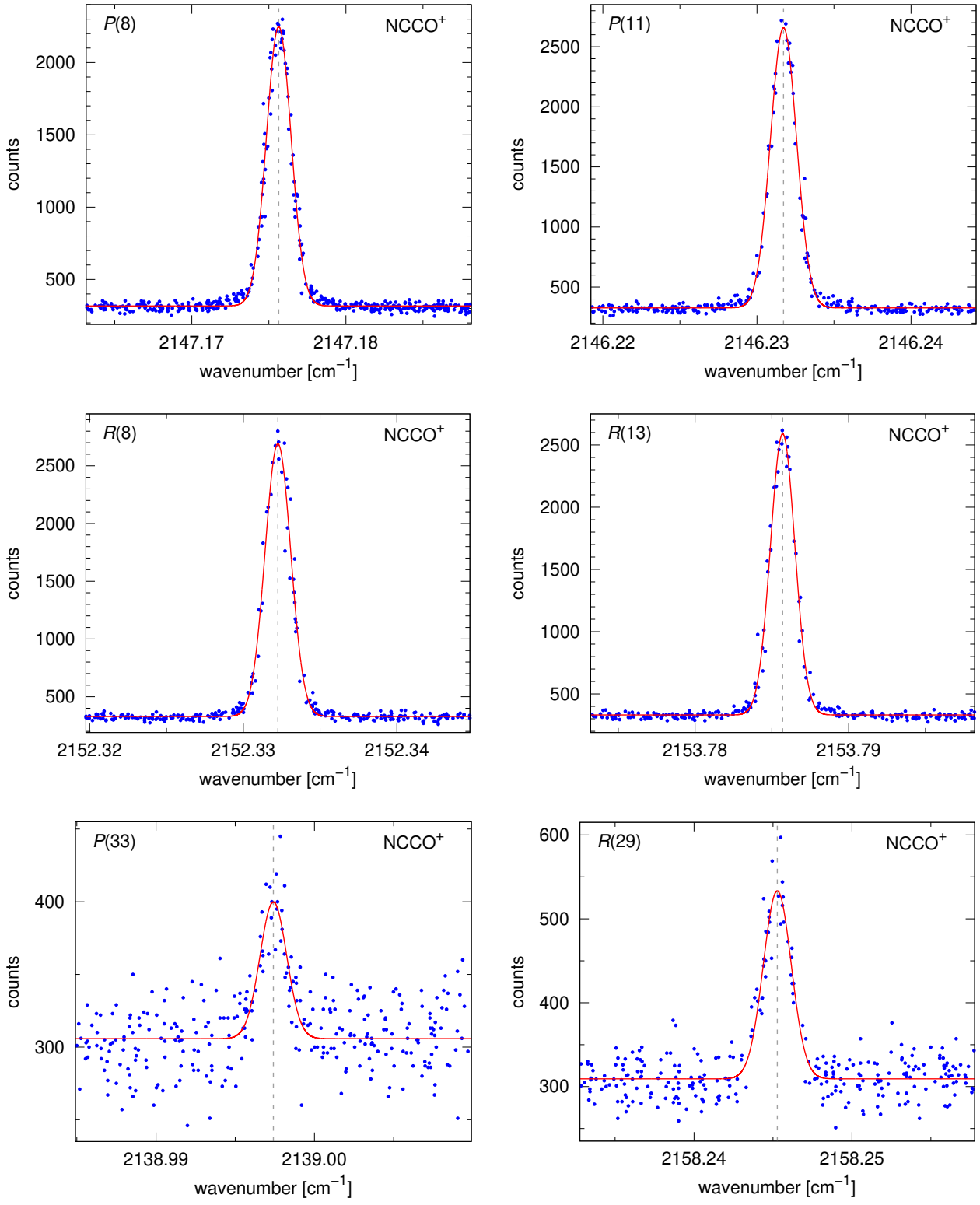

Figure S5: IR LO spectra of ro-vibrational transitions of $NCCO^+$ ν_2 band recorded at COLtrap II. The first two rows show some of the most intense transitions, while the last row shows the weaker transitions at higher J quantum numbers in the P- and R-branches, respectively. All spectra show a spectral range of $0.025\,\mathrm{cm}^{-1}$.

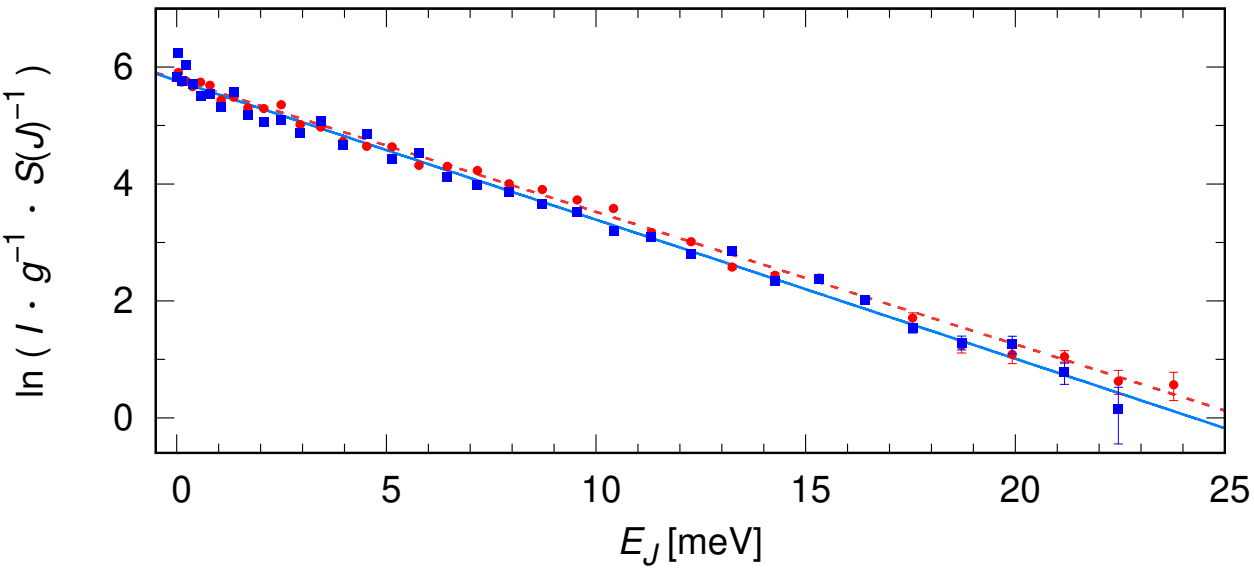

Figure S6: Boltzmann plot of intensities I of P-branch (red dots) and R-branch (blue squares) transitions in the $NCCO^+$ ν_2 band. I is the experimental intensity, g is the multiplicity of the initial rotational state, $S(J)$ is the Hönl-London factor, and E_J is the rotational energy of the molecule in its vibrational ground state. Rotational temperatures, resulting from linear fits, are given by $T_{rot,\,P} = 51.2(9)\,\mathrm{K}$ (red dashed line) and $T_{rot,\,R} = 48.8(16)\,\mathrm{K}$ (blue line). This yields an average rotational temperature of $T_{rot} = 50.0(9)\,\mathrm{K}$.

Global fit file of IR and mmw data

Truncated fit file from output of Pickett's SPCAT program.

						EXP.FREQ. -	CALC.FREQ. -	DIFF. -	EXP.ERR.
1:	34	1	35	0		2138.3124700	2138.3127243	-0.0002543	-0.0002000
2:	33	1	34	0		2138.6557600	2138.6556252	0.0001348	-0.0002000
3:	32	1	33	0		2138.9974100	2138.9974037	0.0000063	-0.0002000
4:	31	1	32	0		2139.3381800	2139.3380592	0.0001208	-0.0002000
5:	30	1	31	0		2139.6777800	2139.6775912	0.0001888	-0.0002000
6:	29	1	30	0		2140.0155900	2140.0159993	-0.0004093	-0.0002000
7:	28	1	29	0		2140.3533600	2140.3532829	0.0000771	-0.0002000
8:	27	1	28	0		2140.6893600	2140.6894415	-0.0000815	-0.0002000
9:	26	1	27	0		2141.0241600	2141.0244748	-0.0003148	-0.0002000
10:	25	1	26	0		2141.3584100	2141.3583821	0.0000279	-0.0002000
11:	24	1	25	0		2141.6913400	2141.6911630	0.0001770	-0.0002000
12:	23	1	24	0		2142.0225800	2142.0228171	-0.0002371	-0.0002000
13:	22	1	23	0		2142.3535600	2142.3533437	0.0002163	-0.0002000
14:	21	1	22	0		2142.6829000	2142.6827425	0.0001575	-0.0002000
15:	20	1	21	0		2143.0110500	2143.0110130	0.0000370	-0.0002000
16:	19	1	20	0		2143.3383200	2143.3381546	0.0001654	-0.0002000
17:	18	1	19	0		2143.6641800	2143.6641669	0.0000131	-0.0002000
18:	17	1	18	0		2143.9887300	2143.9890493	-0.0003193	-0.0002000
19:	16	1	17	0		2144.3128700	2144.3128015	0.0000685	-0.0002000
20:	15	1	16	0		2144.6353100	2144.6354228	-0.0001128	-0.0002000
21:	14	1	15	0		2144.9570400	2144.9569129	0.0001271	-0.0002000
22:	13	1	14	0		2145.2770800	2145.2772712	-0.0001912	-0.0002000
23:	12	1	13	0		2145.5964500	2145.5964973	-0.0000473	-0.0002000
24:	11	1	12	0		2145.9146600	2145.9145906	0.0000694	-0.0002000
25:	10	1	11	0		2146.2317200	2146.2315507	0.0001693	-0.0002000
26:	9	1	10	0		2146.5473000	2146.5473770	-0.0000770	-0.0002000
27:	8	1	9	0		2146.8619300	2146.8620692	-0.0001392	-0.0002000
28:	7	1	8	0		2147.1756400	2147.1756266	0.0000134	-0.0002000
29:	6	1	7	0		2147.4881000	2147.4880489	0.0000511	-0.0002000
30:	5	1	6	0		2147.7994800	2147.7993355	0.0001445	-0.0002000
31:	4	1	5	0		2148.1090000	2148.1094859	-0.0004859	-0.0002000
32:	3	1	4	0		2148.4184800	2148.4184997	-0.0000197	-0.0002000
33:	2	1	3	0		2148.7265400	2148.7263764	0.0001636	-0.0002000
34:	1	1	2	0		2149.0334500	2149.0331154	0.0003346	-0.0002000
35:	0	1	1	0		2149.3386500	2149.3387163	-0.0000663	-0.0002000
36:	1	1	0	0		2149.9463700	2149.9465018	-0.0001318	-0.0002000
37:	2	1	1	0		2150.2487800	2150.2486855	0.0000945	-0.0002000

38:	3	1	2	0	2150.5499900	2150.5497290	0.0002610	-0.0002000
39:	4	1	3	0	2150.8495800	2150.8496321	-0.0000521	-0.0002000
40:	5	1	4	0	2151.1482600	2151.1483940	-0.0001340	-0.0002000
41:	6	1	5	0	2151.4460100	2151.4460145	-0.0000045	-0.0002000
42:	7	1	6	0	2151.7423000	2151.7424929	-0.0001929	-0.0002000
43:	8	1	7	0	2152.0378800	2152.0378289	0.0000511	-0.0002000
44:	9	1	8	0	2152.3322500	2152.3320218	0.0002282	-0.0002000
45:	10	1	9	0	2152.6248100	2152.6250713	-0.0002613	-0.0002000
46:	11	1	10	0	2152.9167100	2152.9169768	-0.0002668	-0.0002000
47:	12	1	11	0	2153.2079800	2153.2077378	0.0002422	-0.0002000
48:	13	1	12	0	2153.4975100	2153.4973539	0.0001561	-0.0002000
49:	14	1	13	0	2153.7857000	2153.7858246	-0.0001246	-0.0002000
50:	15	1	14	0	2154.0733000	2154.0731493	0.0001507	-0.0002000
51:	16	1	15	0	2154.3595700	2154.3593276	0.0002424	-0.0002000
52:	17	1	16	0	2154.6442800	2154.6443591	-0.0000791	-0.0002000
53:	18	1	17	0	2154.9282700	2154.9282431	0.0000269	-0.0002000
54:	19	1	18	0	2155.2108700	2155.2109793	-0.0001093	-0.0002000
55:	20	1	19	0	2155.4921600	2155.4925671	-0.0004071	-0.0002000
56:	21	1	20	0	2155.7730200	2155.7730061	0.0000139	-0.0002000
57:	22	1	21	0	2156.0524800	2156.0522957	0.0001843	-0.0002000
58:	23	1	22	0	2156.3306000	2156.3304356	0.0001644	-0.0002000
59:	24	1	23	0	2156.6075000	2156.6074250	0.0000750	-0.0002000
60:	25	1	24	0	2156.8833500	2156.8832637	0.0000863	-0.0002000
61:	26	1	25	0	2157.1578300	2157.1579512	-0.0001212	-0.0002000
62:	27	1	26	0	2157.4316100	2157.4314868	0.0001232	-0.0002000
63:	28	1	27	0	2157.7039900	2157.7038702	0.0001198	-0.0002000
64:	29	1	28	0	2157.9751400	2157.9751008	0.0000392	-0.0002000
65:	30	1	29	0	2158.2452700	2158.2451782	0.0000918	-0.0002000
66:	31	1	30	0	2158.5141400	2158.5141018	0.0000382	-0.0002000
67:	32	1	31	0	2158.7815200	2158.7818712	-0.0003512	-0.0002000
68:	33	1	32	0	2159.0480700	2159.0484860	-0.0004160	-0.0002000
69:	34	1	33	0	2159.3139400	2159.3139455	-0.0000055	-0.0002000
70:	35	1	34	0	2159.5788100	2159.5782494	0.0005606	-0.0002000
71:	9	0	8	0	82146.19780	82146.19794	-0.00014	0.00800
72:	10	0	9	0	91273.09570	91273.09001	0.00569	0.00800
73:	11	0	10	0	100399.85510	100399.83578	0.01932	0.00800
74:	12	0	11	0	109526.42390	109526.42063	0.00327	0.00800
75:	13	0	12	0	118652.82690	118652.82992	-0.00302	0.00800
76:	14	0	13	0	127779.04790	127779.04904	-0.00114	0.00800
77:	18	0	17	0	164281.72580	164281.73110	-0.00530	0.00800
78:	19	0	18	0	173406.77640	173406.77987	-0.00347	0.00800

```
   79:  20  0 19  0                          182531.53720  182531.55068   -0.01348    0.00800
   80:  21  0 20  0                          191656.03600  191656.02890    0.00710    0.00800
   81:  22  0 21  0                          200780.18940  200780.19991   -0.01051    0.00800
   82:  23  0 22  0                          209904.04350  209904.04907   -0.00557    0.00800
   83:  24  0 23  0                          219027.56670  219027.56175    0.00495    0.00800
   84:  25  0 24  0                          228150.72490  228150.72334    0.00156    0.00800
   85:  26  0 25  0                          237273.52800  237273.51919    0.00881    0.00800
   86:  27  0 26  0                          246395.93470  246395.93467    0.00003    0.00800
NORMALIZED DIAGONAL:
    1   1.00000E+00    2   6.61138E-01    3   3.46793E-01    4   1.00000E+00
MARQUARDT PARAMETER = 0, TRUST EXPANSION = 1.00
                               NEW PARAMETER (EST. ERROR) -- CHANGE THIS ITERATION
   1           199          B      4563.776412(149)         0.000000
   2           111     -alpha2        -17.07451(191)         -0.00000
   3           299         -D        -0.609556(142)E-03    -0.000000E-03
   4            11          E      64444681.23(108)             0.00
 MICROWAVE AVG =        0.000507 MHz, IR AVG =        0.00000
 MICROWAVE RMS =        0.007685 MHz, IR RMS =        0.00020
 END OF ITERATION  1 OLD, NEW RMS ERROR=        0.97644         0.97644
```

Spectra of pure rotational transitions

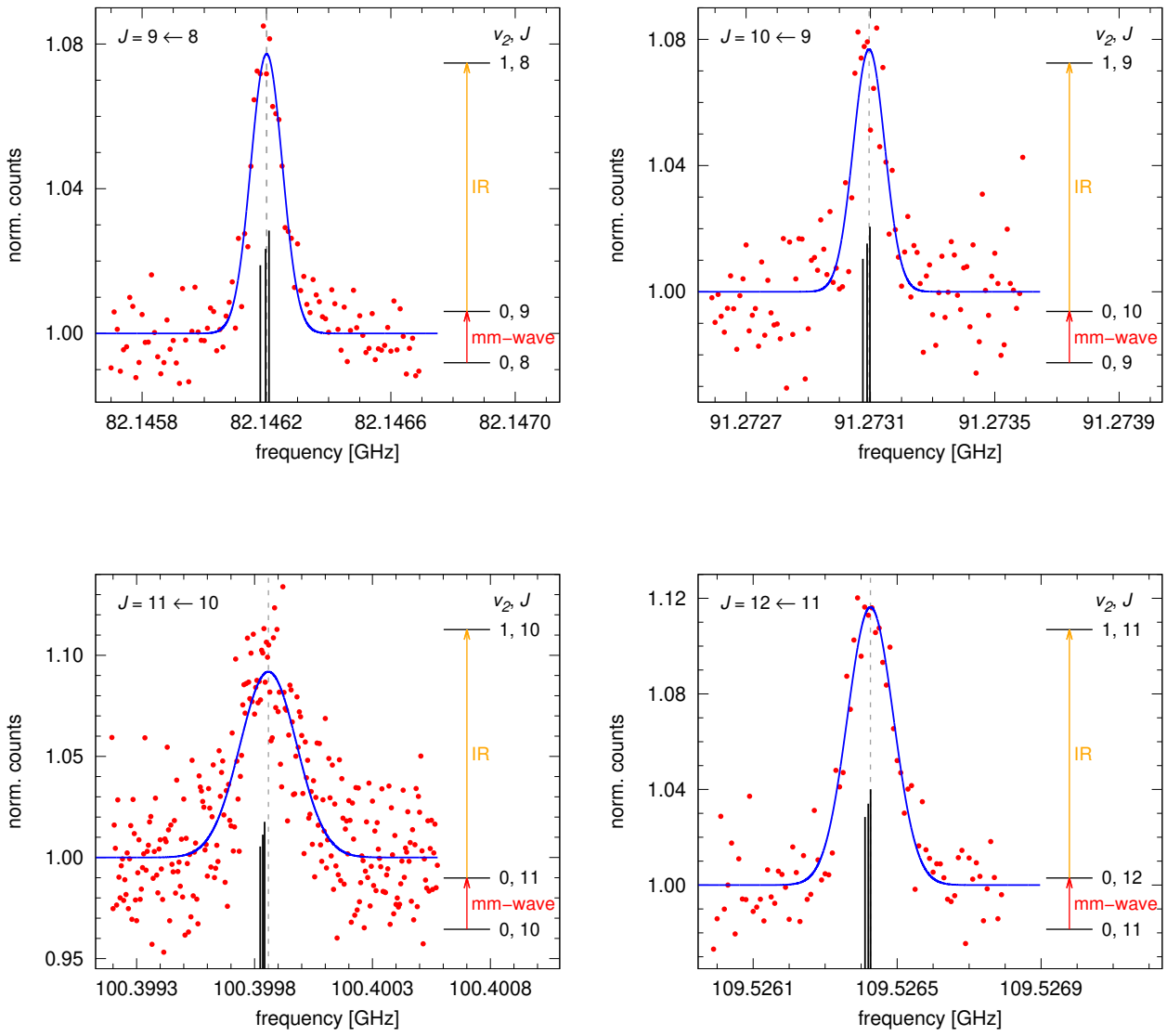

Figure S7: Pure rotational transitions in the ground vibrational state of $NCCO^+$, recorded using a leak-out IR/mmw double resonance scheme. For this recording, the IR laser was stabilized on a ro-vibrational transition of the ν_2 vibrational band (orange arrow) while tuning the mmw frequency in steps of 5 to 10 kHz. Resonant mmw excitation (red arrow) increases the population in the lower quantum state probed by the IR laser, resulting in an increase of the LO signal of up to about 10 %. Normalized counts (red dots) are determined from the ratio of the ion counts in the mmw search window and the counts at an off-resonant reference frequency. Line positions of the mmw fit with calculated hyperfine splitting are shown as black sticks.

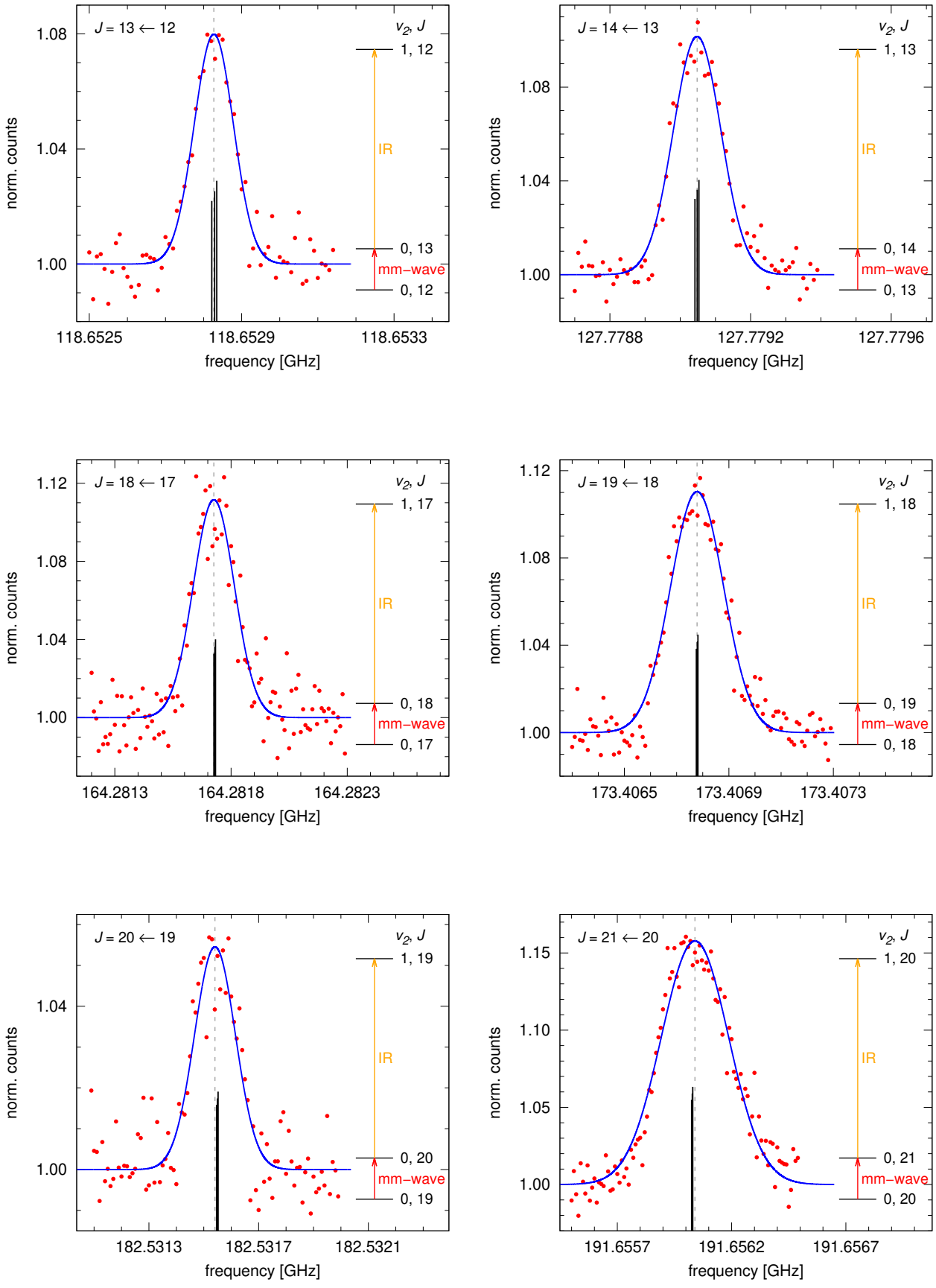

Figure S7 continued.

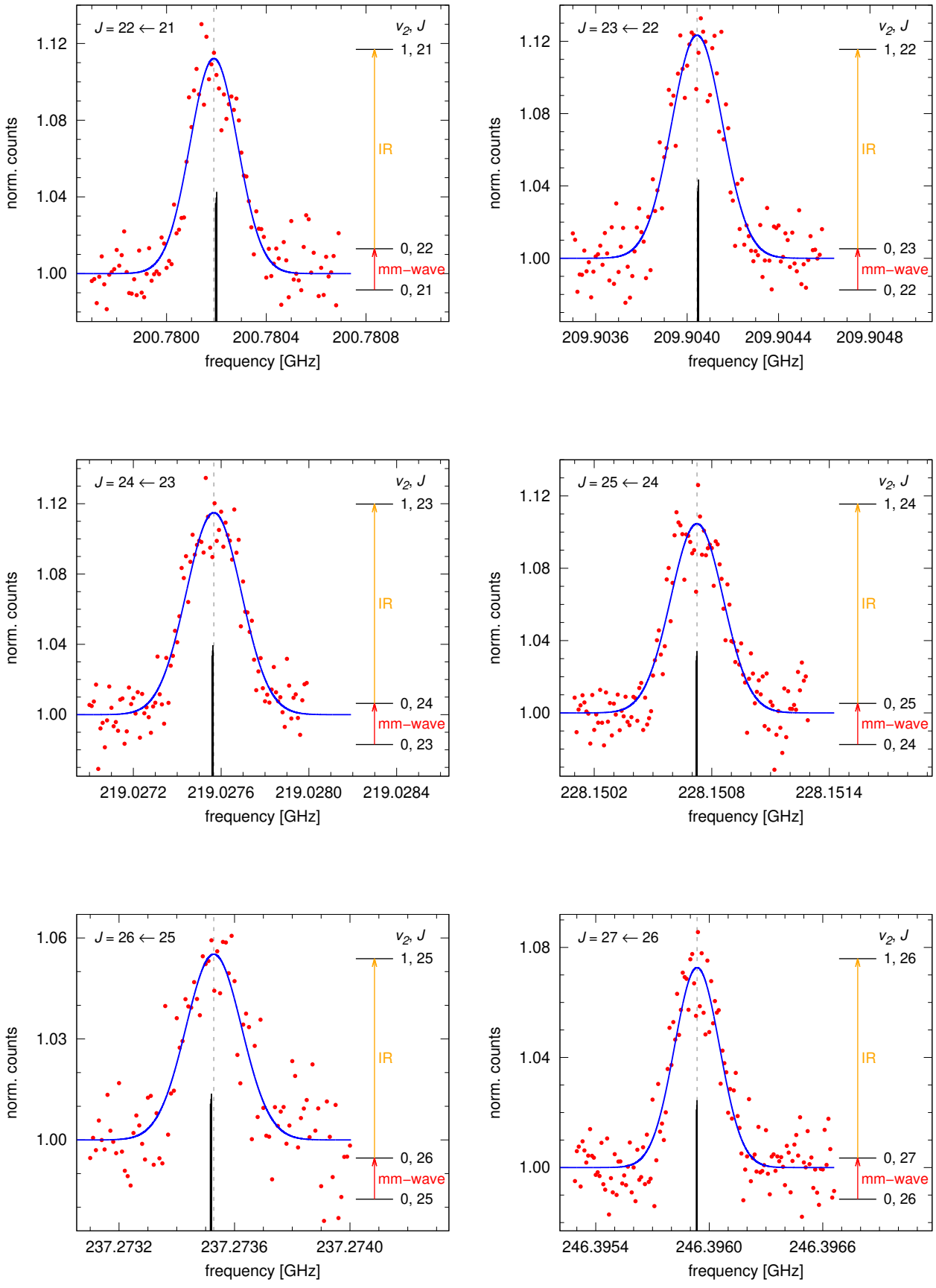

Figure S7 continued.

References

(1) Maki, A. G. High-resolution infrared spectrum of cyanogen. *J. Mol. Spectrosc.* **2011**, *269*, 166–174.

(2) Gerry, M. C. L.; Stroh, F.; Winnewisser, M. The microwave Fourier transform, millimeter-wave, and submillimeter-wave rotational spectra of isocyanogen, CNCN. *J. Mol. Spectrosc.* **1990**, *140*, 147–161.

(3) Bizzocchi, L.; Degli Esposti, C.; Dore, L. Accurate rest frequencies for the submillimetre-wave lines of C_3O in ground and vibrationally excited states below $400\,cm^{-1}$. *Astron. Astrophys.* **2008**, *492*, 875–881.

(4) Amano, T. Submillimeter-wave spectrum of C_3N^- in the extended negative glow and hollow-anode discharges. *J. Mol. Spectrosc.* **2010**, *259*, 16–19.

(5) Amano, T. Extended negative glow and "hollow anode" discharges for submillimeter-wave observation of CN^-, C_2H^-, and C_4H^-. *J. Chem. Phys.* **2008**, *129*, 244305.

(6) Thorwirth, S.; Müller, H. S. P.; Winnewisser, G. The Millimeter- and Submillimeter-Wave Spectrum of HC_3N in the Ground and Vibrationally Excited States. *J. Mol. Spectrosc.* **2000**, *204*, 133–144.

(7) Guarnieri, A.; Hinze, R.; Krüger, M.; Zerbe-Foese, H.; Lentz, D.; Preugschat, D. The millimeter-wave spectrum of ethynylisocyanide (HCCNC). *J. Mol. Spectrosc.* **1992**, *156*, 39–47.

(8) Asvany, O.; Thorwirth, S.; Schmid, P. C.; Salomon, T.; Schlemmer, S. High-resolution ro-vibrational and rotational spectroscopy of HC_3O^+. *Phys. Chem. Chem. Phys.* **2023**,

(9) Gottlieb, C. A.; Apponi, A. J.; McCarthy, M. C.; Thaddeus, P.; Linnartz, H. The rotational spectra of the $HCCCNH^+$, $NCCNH^+$, and CH_3CNH^+ ions. *J. Chem. Phys.* **2000**, *113*, 1910–1915.

(10) Agúndez, M.; Cabezas, C.; Marcelino, N.; Fuentetaja, R.; Tercero, B.; de Vicente, P.; Cernicharo, J. A new protonated molecule discovered in TMC-1: $HCCNCH^+$. *Astron. Astrophys.* **2022**, *659*, L9.

(11) Asvany, O.; Schlemmer, S. Numerical simulations of kinetic ion temperature in a cryogenic linear multipole trap. *International Journal of Mass Spectrometry* **2009**, *279*, 147–155.